Forced response of rotating bladed disks: Blade Tip-Timing measurements

Forced response of rotating bladed disks: Blade Tip-Timinig measurements

G. Battiato[a,*], C. M. Firrone[a], T. M. Berruti[a]

[a]*Dipartimento di Ingegneria Meccanica e Aerospaziale, Politecnico di Torino, Corso Duca degli Abruzzi, 24, 10129 Torino*

Abstract

The Blade Tip-Timing is a well-known non-contact measurement technique for the identification of the dynamic properties of rotating bladed disks. Even if it is an industry-standard technique its reliability has to be proved for different operation conditions by the comparison with other well established measurement techniques. Typically the strain gauges in conjunction with a radio telemetry is used as reference.

This paper aims at evaluating the accuracy of a last generation Tip-Timing system on two bladed dummy disks characterized by different geometrical, structural and dynamical properties. Both the disks were tested into a spinning rig where a fixed number of permanent magnets, equally spaced around the casing, excites a synchronous vibrations with respect to the rotor speed.

A new set up of the optical sensors was adopted for the Tip-Timing system. Due to the presence of shrouds, it was avoided that the probes look radially inward at the blade tips as in the most common configurations. The probes are optical laser sensors pointing at the leading and trailing edges locations where the blade experiences the greatest magnitude of displacement.

Besides the typical Blade Tip-Timing application aimed at identifying the dynamical properties of each blade, an original method is here proposed to identify the operative deflection shape of the disk by experimentally observing

*Corresponding author
Email address: giuseppe.battiato@polito.it (G. Battiato)

the nodal diameters. The method is applicable when a small mistuning pattern perturbs the ideal cyclic symmetry of a bladed disk.

Keywords: Blade Tip-Timing, Vibrations, Bladed Disk, Spinning Tests, Mistuning

1. Introduction

Vibrations in turbomachinery could reduce the blades fatigue life by increasing the risk of crack formation. In this frame the blade health monitoring represents an important challenge in order to prevent unexpected blade failures. Traditionally, the rotor blade vibrations have been detected using the strain gauges, which still represent nowadays the most reliable measurement system. However, the main disadvantage of using the strain gauges is that they cannot be used in the engine in service since they need to be stuck on the blade airfoil. For this reason in the last years of blades monitoring, the non-contact measurement technique Blade Tip-Timing (BTT) has gained ground. The BTT technique is based on the analysis of the arrival times related to the blade passages under a set of stationary sensors [1, 2]. In the standard cases the BTT sensors are mounted on the casing, oriented radially in order to detect the blade displacements at the tip [3]. One of the main advantages of the BTT is that, besides of being non-contact and usable on a working engine, all the blades are monitored during the rotation. It is therefore possible to identify if one blade vibrates more than the others (for typical mistuning problems). The last generation industry-standard BTT systems process the arrival times by using indirect [4, 5, 6, 7] or direct [5, 8, 9, 10] identification methods in order to determine the modal parameters characterizing the vibrating blade. A verification on the correctness of the obtained parameters represents a due step in order to consider the BTT measurement system as reliable. Different authors have demonstrated a good correlation between measurements from BTT and strain gauges for both real [3] and controlled [11] operation conditions, in the case where the displacements are measured at the blade's tip using the standard radial sensors positioning.

The present paper explores the capability of the BTT technique as a measurement method useful not only for the determination of the amplitude and frequency of each single blade, but also for the identification of the deformed shape of the measured mode. In this frame an extensive experimental campaign was performed on two disks. The first is a dummy disk with a simple geometry of a flat plate, characterized by blade bending vibration modes along the disk axial direction. The second is a dummy disk designed to simulate a dynamic behavior closer to a real turbine disk where the blades are connected each other at the tip by an outer ring.

Two main issues are described in the paper. The first issue is the validation on both the disk geometries of a new set up of the optical sensors in the BTT technique, the *beam shutter* or *beam interrupted* configuration. This probe arrangement allows only one set of probes working both as sender and receiver of the reflected beam. The measurement results were validated agaist the measurements of the strain gauges glued on the same blades measured by the BTT system. The second issue is the proposal of an original method to identify, from the response data of all the blades, the nodal diameter number of the main disk response mode. The method does not work when the mistuning is so large to destroy completely the cyclic symmetry, but only when a small mistuning is present. It is here proved, in fact, that the small mistuning induces a particular modulation of the blades response amplitude. It is shown in different cases, both on experimental and simulated results, that the number of lobes of this modulation is related to the number of the nodal diameter of the main disk response mode.

2. The spinning test rig

The two dummy disks were tested in a laboratory spinning rig under vacuum conditions [12]. As shown in Fig. 1 (a) the test rig has a vertical axis with two cylindrical protective structures (1) and (2) coaxial to the rotating shaft, which is positioned under the floor. On the top of the shaft a flange allows the disk

accommodation (3). The cylinder (1) also supports two static rings (Fig. 1 (b)): Ring 1 keeps in a fixed position a set of permanent magnets, which are used to excite the rotating disk, and Ring 2 hold the BTT laser sensors.

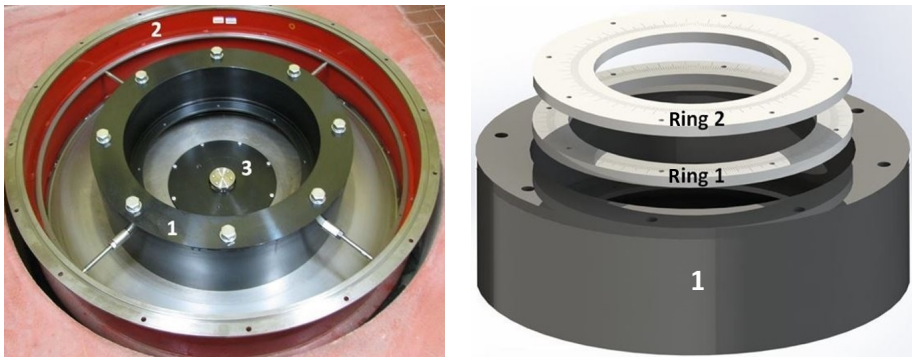

(a) (b)

Figure 1: The spinning rig (a), static rings for magnets and laser sensors (b).

2.1. The dummy disks

The dummy disk 1 (Fig. 2 (a)) is an aluminium disk with a simple geometry of a flat plate where each blade has the shape of a cantilever beam. The disk 1 has 12 blades whose length and width are 150 mm and 25 mm respectively. The thickness and the outer diameter of the disk are 5mm and 400 mm. A cylindrical magnet (5 mm diameter, 5 mm height) is glued in a housing drilled at the tip of each blade.

The dummy disk 2 (Fig. 2 (b)) was designed to have a dynamic behaviour closer to a real turbine disk. The blades are connected to each other at the tips by an outer ring, as in the case of shrouded blades. It is a single piece made of ferromagnetic steel AISI 460 in order to allow the magnetic interaction between the permanent magnets and the blade airfoils. It has 32 profiled blades whose length and aspect ratio are respectively 100 mm and 7.31. The disks outer diameter and axial height are 630 mm and 20 mm.

(a) (b)

Figure 2: The dummy disk 1 (a), the dummy disk 2 (b).

2.2. The excitation system

The excitation system in the spinning test rig uses cylindrical permanent magnets (diameter 18 mm, height 10 mm, grade N52). The magnets are mounted in equally spaced positions on the static ring facing the rotating test article (Ring 1 in Fig. 1 (a)). A graduated scale impressed on the ring upper surface is used to fix the magnets at the right angular positions [12].

Several supporting rings with different inner diameter are available in order to guarantee the correct radial positioning of the permanent magnets. Each magnet is glued on the tip of a screw that allows the regulation of the axial gap with respect to the disks blades. Six of the magnets were instrumented with force transducers that measure the force in axial direction during the tests [12].

The number of magnets used in a specific test must be equal to the main engine order (EO) characterizing the excitation force that should be simulated. The main engine order EO_m^1 can be defined as the fist not-null harmonic index resulting from the Fourier transform of the excitation force. In general for m equally spaced magnets, the EO pattern exciting the disk is defined as follows:

$$EO_m^i = i \cdot m, \qquad \forall\ i = 1, 2, 3, \ldots \tag{1}$$

A modal shape corresponding to a certain nodal diameter number (ND) can be excited by different EO according to the following relationship, where N_b is

the number of the disks blades:

$$EO = jN_b \pm ND, \qquad \forall\ j = 0, 1, 2, 3, \ldots \tag{2}$$

The excitation frequency is related both to the EO and to the rotational speed n by the following equation, where n is given in rpm and f_{exc} in Hz:

$$f_{exc} = \frac{EO \cdot n}{60} \tag{3}$$

From the Eq. 3 it can be seen that with high EO values the bladed disk can be excited at the same excitation frequency f_{exc} with lower values of the rotational speed n.

2.3. The strain measurement system

The two dummy disks were instrumented by means of strain gauges. For both the disks the identification of the strain gauge positions came out from their FE modal analyses in cyclic symmetry conditions. Areas of high strains and low strain gradients were identified as the best locations for strain gauges. The strain gauges signals were acquired through a telemetry system.

(a) (b)

Figure 3: Strain gauge at the blade root of the dummy disk 1 (a), strain gauge at the back of the airfoil of a dummy disk 2 blade (b).

For the dummy disk 1 the strain gauges were attached at the two sides of the blade root (Fig. 3 (a)). This position was chosen in order to measure the

out of plane bending mode (1F) belonging to the first modal family. Each strain gauge is composed by a single grid (1.52 mm $\times$ 3.05 mm, grid resistance 350 Ω). The two grids at the two sides of the blade were connected together with a half bridge. For the dummy disk 2 the strain gauge was attached on the back of the blade airfoil (Fig. 3 (b)). The selected area is not affected by strain gradients for both the flap-restricted (1FR) and torsional (1T) mode shapes belonging to the second and third modal family respectively. The strain gauge is a tee rosette (grid resistance 350 Ω) composed by two separate grids (1.52 mm $\times$ 1.78 mm) with perpendicular axes. The two grids were connected together with a half bridge. The strain gauges measurement chain was verified by means of a static test on the dummy disk 1. The static test on the instrumented blade consisted in measuring the bending strain at the blade root due to calibrated masses positioned on its free end. Three static tests corresponding to three different dead masses were performed and the measured strains were compared to the corresponding numerical strains determined by means of the static FE analysis.

Mass	*Strain Gauge*	*FE model*
kg	$\mu\epsilon$	$\mu\epsilon$
0.76	130.23	130.19
1	169.30	169.27
1.99	342.32	342.25

Table 1: Experimental and numerical strains for the static tests on the dummy disk 1.

The results listed in Table 1 show the reliability of the strain gauges, which can be used as a reference measurement system for the validation of the BTT technique.

3. The Blade Tip Timing mearurement system

The BTT technique uses a set of non-contact sensors constrained to the casing and facing the rotating disk[1, 2, 3]. This technique is based on the measurement of the *Times-of-Arrival* (ToA) of each blade under each of the stationary sensor. From the analysis of the ToA the dynamic properties of each blade, i.e. the resonance frequency, the vibration amplitude and the modal damping, can be determined. The BTT has two main advantages over the strain gauges:

- it is a non-contact measurement system that does not affect the dynamic behavior of the blade;
- it allows the measurement of all the blades of the disk, while the strain gauges are usually attached only to some of the blades.

The BTT system used in this study is a last generation system with laser optical probes. For the dummy disks 1 and 2 all the tests were performed by employing five optical laser sensors for detecting the blades vibrations. An additional sensor (1/rev sensor) that measures the rotational speed was used a reference for the other sensors

3.1. The beam shutter method and the sensor positioning

The standard BTT measurement approach is based on sensors that are positioned in radial direction in order to measure the blade displacement at the tip. In this study a new sensor configuration called *beam shutter* or *beam interrupted* was tested. The probes position in the beam shutter configuration for the dummy disks 1 and 2 is shown in Fig. 4.

A set of sender-receiver optical laser sensors with lenses was used for both the disks. Each sensor was mounted above the disk and produces a laser beam that was collimated on a reflective tape stuck on a stationary surface placed under the disk. When the disk rotates the passing blade acts as a shutter, blocking

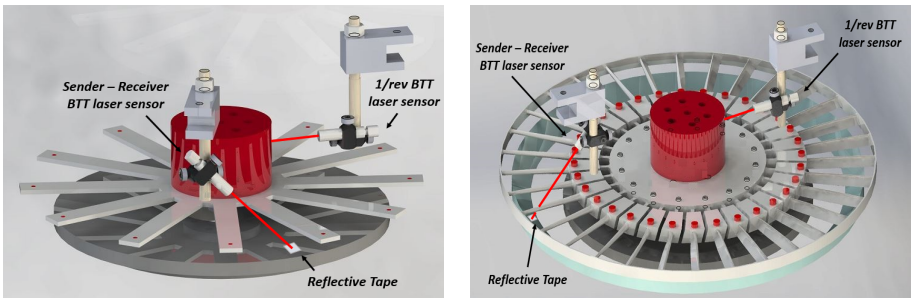

(a) (b)

Figure 4: Beam shutter configuration for the dummy disk 1 (a), and the dummy disk 2 (b).

the returning light towards the sender-receiver sensor. The system was set up in order to detect the ToA of the leading or the trailing edge of the blade.

The sensors were installed at the same distance from the disk center. The relative circumferential position of the sensors was chosen in both cases by means of an optimization tool, which avoids the aliasing effect in the measurement of the travelling wave characterizing the vibrating disk. The optimization tool requires as input the number of sensors, the expected engine orders and the number of blades.

3.2. The BTT data post-processing

The data were post-processed by using a fitting method called *Circumferential Fourier Fit* (CFF) [13]. This method requires three or more sensors installed on the same chord-wise position. Assuming a certain response order, corresponding to the selected EO, for each averaged rpm a sinusoidal wave is fitted to the data [5, 8, 9, 10]. In detail each blade is assumed to vibrate according to a sinusoidal wave. The equation of the blade motion seen by the k^{th} sensor is:

$$y_k(\omega) = c + A(\omega) \cdot \sin\left(2\pi \cdot EO \cdot f \cdot t + \Phi(\omega)\right) =$$

$$= c + A(\omega) \cdot \sin\left(EO \cdot \theta_k + \Phi(\omega)\right) \tag{4}$$

where $A(\omega)$ and $\Phi(\omega)$ are the amplitude of vibration and phase at a certain frequency ω and θ_k is the angular position of the k^{th} sensor. For a given blade at each frequency (that is each value of the rotation speed) the displacement $y_k(\omega)$ is measured by each the k^{th} sensor. Eq. 4 is then written for each sensor and the terms $A(\omega)$, $\Phi(\omega)$ and c are calculated by a least square process if more than 3 sensors are involved in the measurements. The amplitude $A(\omega)$ can then be plotted versus the rotation speed as shown later in Fig. 8.

4. The results comparison method

In order to verify the accuracy of the BTT, the vibration parameters detected by the BTT system were compared to the same parameters coming from the strain gauges connected to the telemetry system. Simultaneous measurements with BTT and strain gauges were performed for a certain set of vibrating modes characterizing the dummy disks. While the comparison in terms of resonance frequencies is straightforward and requires a fast data processing, the comparison in terms of vibration amplitudes is a more demanding task. Indeed, it requires a finite element (FE) modal analysis of the disks, since the strain gauges system measures strains (ϵ_{SG}), while the BTT measures displacements (u_{BTT}). By the FE model the parameter $K_{mod} = u_{mod}/\epsilon_{mod}$ can be calculated, where:

- u_{mod} is the modal displacement of the node corresponding to the laser position on the blade in the same direction of the displacement detected by the BTT;
- ϵ_{mod} is the modal strain in the area corresponding to the strain gauges position in the same direction of the strain detected by the strain gauges.

The same parameters can be defined for the physical measured quantities u (displacement of the blade at the BTT laser position) and ϵ (strain at the strain gauges position) $K_{phy} = u/\epsilon$. Since the two disks can be considered linear and their responses give well separated modes, the following relationship should be

satisfied:

$$K_{phy} = K_{mod} \quad \Rightarrow \quad \frac{u}{\epsilon} = K_{mod} \tag{5}$$

The displacement of the blade corresponding to the strain measurement from Eq. 5 can be determined as:

$$u_{SG} = K_{mod} \cdot \epsilon_{SG} \tag{6}$$

Since the FE model was tuned previously by the strain gauge measurements (see Table 1) the obtained parameter u_{SG} is considered as reference for the displacement value measured by the BTT system u_{BTT}.

5. Results on the dummy disk 1

In order to predict the natural frequencies and the mode shapes a FE dynamic calculation in cyclic symmetry conditions was performed. In Fig. 5 (a) the natural frequencies of the dummy disk 1 are plotted against the NDs (FreND diagram) resulting in the first modal family called 1F. Each black circle in Fig. 5 (a) refers to an out of plane bending mode of the blade when the disk vibrates according to a certain ND. From the numerical Campbell diagram in Fig. 5 (b) the rotation speeds at which the resonances occur can be estimated. The modes corresponding to $ND = 5$ and $ND = 6$ were chosen to be tested.

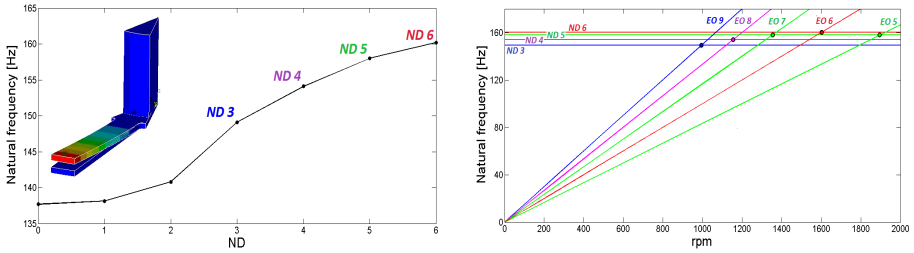

(a) (b)

Figure 5: Numerical FreND diagram for the dummy disk 1 (a), numerical Campbell diagram for the dummy disk 1 (b).

The mode with $ND = 6$ was excited by an harmonic force with $EO = 6$. In

order to avoid high operation speed, it was chosen to excite the mode with $ND = 5$ by an harmonic force with $EO = 7$ instead of a $EO = 5$ according to Eq. 2.

5.1. Displacement measurement with the Blade Tip-Timing

The dummy disk 1 has out of plane bending mode shape (the blade vibrate along the axial direction). In order to obtain a configuration where the optical beam is interrupted by the blade during an out of plane vibration, the sensors must be positioned with an angle with respect to the disk plane as shown in Fig. 4 (a). Each sensor was then tilted by an angle, which is 45° with respect the plane containing the undeformed disk. This particular angle of the sensors allows the BTT system to see an axial displacement as it was tangential as shown by the scheme of the blade interrupting the laser beam in Fig. 6. The time interval between the detected ToA and the theoretical undeformed position (Δt in Fig. 6) corresponds to the apparent tangential displacement that is equal to the actual axial displacement.

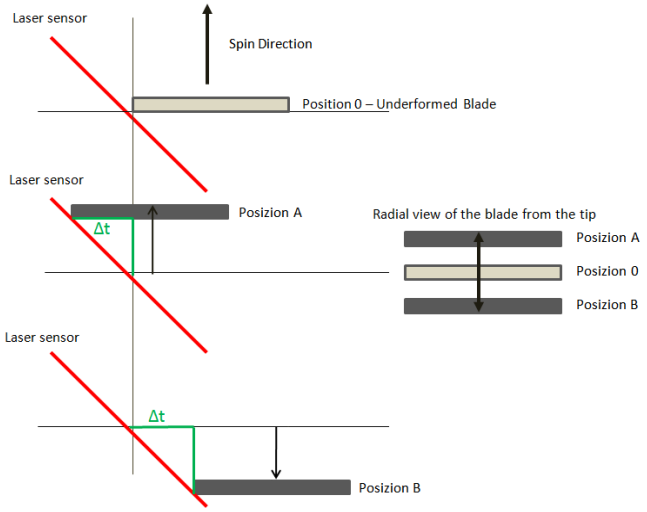

Figure 6: Beam shutter working principle adopted for detecting the out of plane vibration modes for the dummy disk1.

5.2. Preliminary test

A preliminary rotating test was performed to identify the real resonance frequencies. A single magnet was mounted on the test rig so that the disk could be excited simultaneously by means of an infinite number of harmonic excitations ($EO_1 = 1, 2, 3, \ldots$). The test was planned in order to investigate the speed range 600 - 2600 rpm.

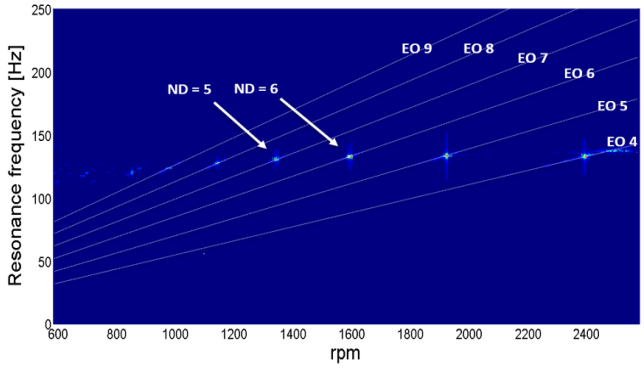

Figure 7: Experimental Campbell diagram for the dummy disk 1.

From the strain gauges time signal the experimental Campbell diagram (Fig. 7) was processed using Matlab. The natural frequencies for the modes corresponding to $ND = 5$ and $ND = 6$, which were determined by reading the y-axis values of the white points, are listed in Table 2.

EO	ND	n_{res}	f_{res}
-	-	rpm	Hz
7	5	1356	158.2
6	6	1591	159.1

Table 2: Dummy disk 1 resonance frequencies for the mode shapes with $ND = 5$ and $ND = 6$ (out of plane bending modes).

5.3. Test campaign

The test campaign was performed for the modes that were excited by the EOs determined from Eq. 2 for $j = 1$. A single permanent magnet was adopted for the excitation. A gap of 7 mm between the permanent magnet and those glued at the blades' tips was set for all the tests. Strain and displacement were acquired simultaneously for two speed ranges including the values of n_{res} at which the resonances occur. The main tests parameters are listed in Table 3.

EO	*ND*	n-range
-	-	rpm
7	5	1300 - 1400
6	6	1550 - 1650

Table 3: Test campaign for the dummy disk 1.

The test campaign was repeated 3 times. For each test a linear sweep in speed with an acceleration of 0.3125 Hz/s was performed.

5.4. The comparison BTT - strain gauges

The strain gauges and BTT data were processed for each of the studied modes. For the strain gauges data processing the same procedure employed for the preliminary test was adopted.

The measured displacement amplitude in resonance condition and the corresponding resonance frequencies were averaged over the three acquisitions. The measured values showed high repeatability (standard deviation $\bar{\sigma} < 0.13\%$ of the mean value). Table 4 lists the displacement amplitudes and the natural frequencies detected both by stran gauges (SG) and by the BTT system. The parameters e_f, e_u represent the percentage differences between the resonance frequencies and vibration amplitudes detected by the strain gauges and the BTT:

$$e_f = \frac{\bar{f}_{SG} - \bar{f}_{BTT}}{\bar{f}_{SG}} \cdot 100 \qquad (7)$$
$$e_u = \frac{\bar{u}_{SG} - \bar{u}_{BTT}}{\bar{u}_{SG}} \cdot 100$$

From Table 4 it can be noted that the difference in terms of resonance frequency is negligible (e_f is lower than 0.5%). The difference in terms of resonance amplitude is also very low, the paramer e_u is less than 2%.

ND	$\bar{f}_{SG}$	$\bar{f}_{BTT}$	e_f	$\bar{u}_{SG}$	$\bar{u}_{BTT}$	e_u
-	Hz	Hz	%	μm	μm	%
5	158.0	158.0	0	1662.23	1631.48	1.88
6	159.3	160.2	0.44	2298.75	2275.60	1.02

Table 4: BTT - strain gauges comparison for the dummy disk 1.

5.5. From a single blade measurement to the global disk response

One of the advantages of the BTT system over the strain gauges is that every blade can be measured while, if strain gauges are used, only the response of the instrumented blades are detected. However, the measurement of the blades as independent structures having their own amplitude and resonance frequency does not allow to catch the global disk behavior in terms of nodal diameter of the travelling response. A preliminary calculation of the Campbell diagram (Fig. 5 (b)) obtained by means of a FE model of the bladed disk can be useful to estimate the ND number of the response. When a resonance is detected by the system, the corresponding rotation speed is the input value to the Campbell diagram to verify the presence of a crossing 'ND natural frequency - EO line that satisfies' Eq. 2. Instead of estimating the nodal diameter number from the Campbell diagram, it is here analyzed how it can be obtained directly by the BTT measurements.

For the studied mode shapes ($ND = 5$ and $ND = 6$) the forced responses post-processed by the BTT of all the blades are reported in Fig. 8. If the

dummy disk were a perfectly tuned disk, i.e., all the hypothesis for a cyclically symmetric body were respected in terms of geometry, material properties and constraints, the forced response of each blade should be the same. It can be observed that this holds for the stationary *Operating Deflection Shape* (ODS) with $ND = 6$ (Fig. 8 (a)), where the response peak of each blade occurs at the same rotation speed with the same amplitude. This is not the case of the travelling ODS with $ND = 5$ (Fig. 8 (b)), where the maxima amplitudes occur at slightly different rotation speed and their envelope appears as a spatial wave along the blade number. The same spatial wave can be observed along the blade number at a given rotation speed.

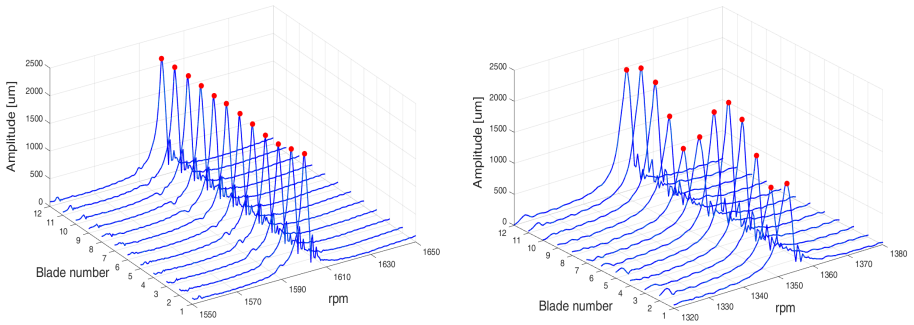

(a) (b)

Figure 8: Experimental forced responses for the twelve blades of the dummy disk 1 detected by the BTT in the case of $ND = 6$ (a) and $ND = 5$ (b) mode shape.

This phenomenon was already observed in [14] where a test campaign on a not rotating dummy bladed disk excited by an EO travelling force produced by electromagnets was performed. In that case it was demonstrated that due to the presence of a small mistuning of the disk the spatial wave for a given excitation frequency had a number of lobes equal to two times the number of the ODS nodal diameters. In detail, for a dummy bladed disk with 24 blades, a four lobe envelope of the blades amplitude was observed for an ODS with $ND = 2$ and a six lobe envelope was observed for an ODS with $ND = 3$. In the case of Fig. 8 (b), where the ODS with $ND = 5$ is shown, ten lobes are

expected in the spatial wave. As it is shown in the same figure, the envelope of the maxima amplitudes clearly shows two lobes instead of ten. This can be explained considering the aliasing effect generated by the poor discretization of a spatial wave with 10 lobes along the 12 blades. In detail, assuming N_b as the number of blades, L_{exp} the number of lobes of the expected spatial wave and L_s the number of lobes of the spatial wave sampled by the blades, two cases can occur:

- if $L_{exp} \leq N_b/2$, the modulated spatial wave can be well recognized as wave with L_{exp} lobes. In this case $L_{exp} = L_s$ and no aliasing occurs;

- if $L_{exp} > N_b/2$ (Fig. 8 (b)) , the number of blades is not large enough to correctly discretize a spatial wave with L_{exp} lobes. In this case aliasing occurs and the observed spatial wave has a number of lobes L_s which satisfies the following relationship:

$$L_{exp} = jN_b \pm L_s, \qquad \forall\ j = 0, 1, 2, 3, \ldots \tag{8}$$

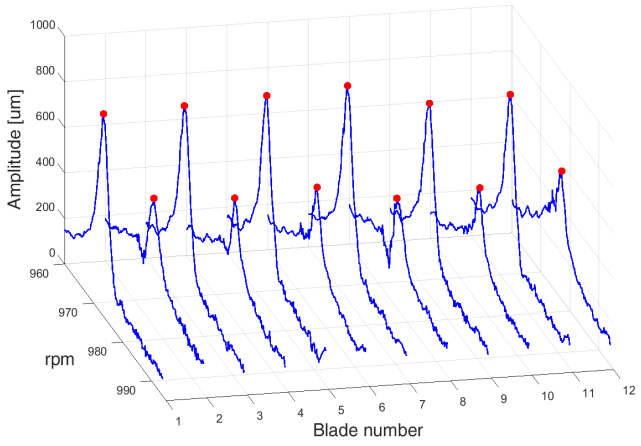

Figure 9: Experimental forced responses for the 12 blades of the dummy disk 1 detected by the BTT in the case of the $ND = 3$ mode shape.

In order to confirm the experimental observation in a case where no aliasing occurs, the measurement was performed also in the range of the natural

frequency corresponding to $ND = 3$: the ODS, plotted in Fig. 9, shows as expected a spatial wave with six lobes.

In the next section a simplified lumped parameters system is used to demonstrate that the appearance of the spatial waves. The number of lobes, double with respect to the number of nodal diameters, is strictly associated to the existence of two repeated modes in the presence of small mistuning. This happens when $1 < \mathrm{ND} < N_b/2$ if N_b is even. When $ND = 0$ or $ND = N_b/2$ (for an even number of blades) only one mode is present and the spatial wave does not appear. This is confirmed by the observation of the flat ODS corresponding to $ND = N_b/2 = 6$ (Fig. 8 (a)).

5.6. An analytical model to explain the blade row response

In order to explain the appearance of the spatial wave, a simple analytical model of a lumped parameter disk was built. The disk has 12 sectors, each one with one degree of freedom coupled by means of a springs. The sectors are the same, therefore the disk is tuned and 12 identical forced response amplitudes are obtained as shown in Fig. 10 (a) with $ND = 3$.

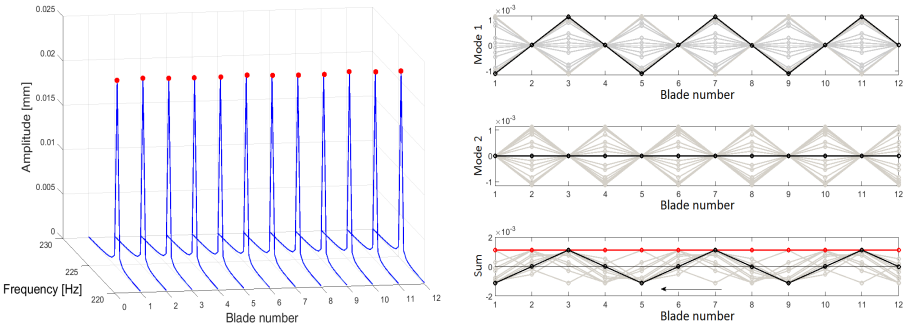

(a) (b)

Figure 10: Numerical forced responses (a) and ODS (b) for a cyclic symmetric mode shape with $ND = 3$.

In Fig. 10 (b) the two repeated mode shapes multiplied by their participation factors are plotted at resonance for different time instants. Under a travelling

excitation force the repeated mode shapes are orthogonal not only in space but also in time. The orthogonality along the blade number is clearly visible, while the orthogonality in time is indicated with the two black solid lines: when the first mode is at its maximum amplitude the second mode is at its neutral position. The linear combination of the two modes produces a travelling ODS (lower subplot of Fig. 10 (b)). The peak envelope of the blade amplitudes is a straight line (red) since the disk is tuned.

A random mistuning was then added to the disk model, this leads to a splitting of the frequencies of the repeated modes of about 0.7 % of the tuned natural frequency. As it can be seen in Fig. 11 (a), the consequence of this is that the sum of the two modes, having slightly different frequencies and amplitudes, gives an ODS where the final peak envelope is no more a straight line. The results is a spatial wave with six lobes for a $ND = 3$ response. This model shows that the presence of the spatial wave, seen in the experimental forced responses (Fig. 8 (b) and Fig. 9), is due to a small mistuning that causes the splitting of the frequencies of the two orthogonal modes associated to the same ND.

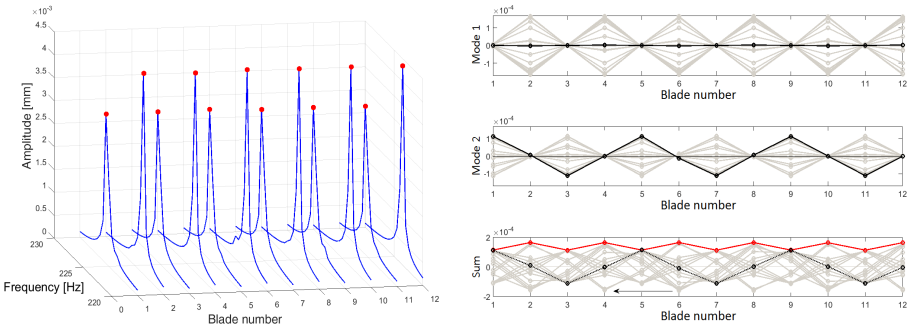

(a) (b)

Figure 11: Numerical forced responses (a) and ODS (b) for a mistuned mode shape with $ND = 3$.

By using the same model the cases of Fig. 8 (a) and (b) can also be simulated. Fig. 12 (a) shows the simulated forced responses in the case where a mode

corresponding to $ND = 6$ is excited in a small mistuned numerical model. This example corresponds to the experimental case of Fig. 8 (a). It can be seen in the simulation (Fig 12 (b)) that the second mode does not exist and then it cannot give rise to a spatial wave with the first mode.

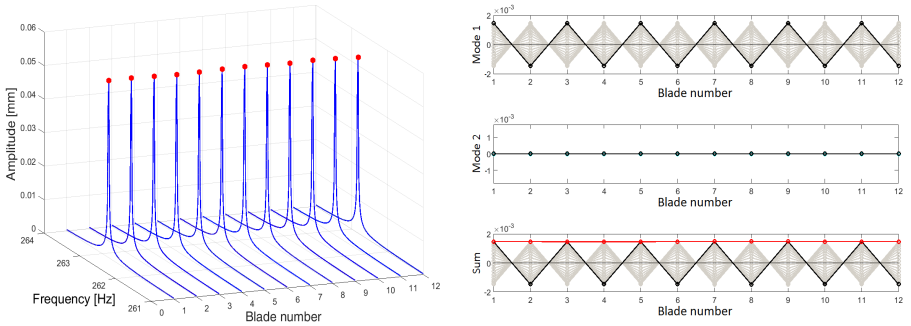

(a) (b)

Figure 12: Numerical forced responses (a) and ODS (b) for a mistuned mode shape with $ND = 6$.

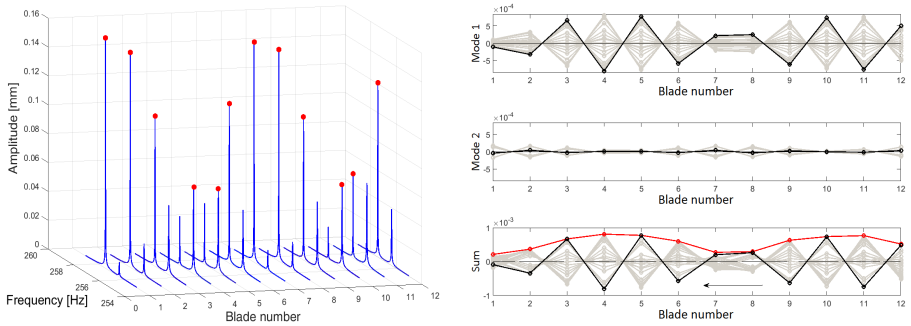

(a) (b)

Figure 13: Numerical forced responses (a) and ODS (b) for a mistuned mode shape with $ND = 5$.

Fig. 13 (a) shows the result of the simulation for an ODS with $ND = 5$. This example corresponds to the experimental case of Fig. 8 (b). It can be seen that the simulated forced responses shows a modulated spatial wave with two

lobes due to aliasing as in the experiments. It can then be concluded that the presence of small mistuning, which is expected to be present in the real disks, can be useful to experimentally observe the nodal diameters of the response from the measurements of all the blades detected by the BTT system.

6. Results on the dummt disk 2

The dummy disk 2 has been built to reproduce a bladed disk dynamics similar to a real turbine disk. Measurements on this disk allow testing the capability of the BTT system to give accurate results even on a disk with a more complex dynamics. The FE dynamic calculation on the dummy disk 2 showed that the modes belonging to the first three modal families are characterized by the flap (1F), flap restricted (1FR) and torsional (1T) blade modes shapes respectively. The FreND diagram corresponding to the 1^{st}, 2^{nd} and 3^{rd} modal family is shown in Fig. 14. From the FE analyses on the dummy disk 2 the high strain locations on the blade airfoil, for the 1FR and 1T mode shapes, were chosen for the strain gauges installation (middle of the blade airfoils, Fig. 3 (b)). It was then decided to excite the 1FR and 1T mode shapes for a certain ND.

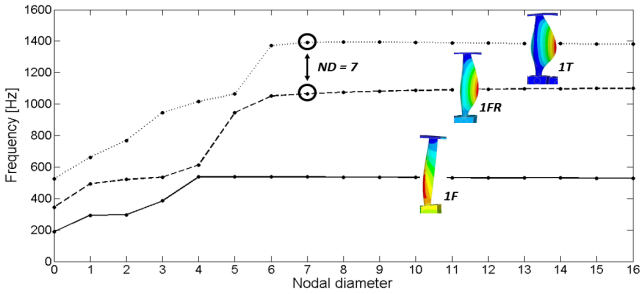

Figure 14: Numerical FreND diagram for the dummy disk 2.

6.1. Preliminary hammer test

A preliminary hammer test was performed to detect the modal parameters of the disk in stationary static conditions (not rotating). In order to have the same

constraints with the shaft as during the rotation, the disk was kept mounted on the spinning rig during the hammer test. The response of each blade was measured by a laser scanner in a location close to the selected location used by the BTT laser probes. It was observed that the cleanest disk responses for both the 1FR and 1T modes occurred for $ND = 7$ that is at 1029 Hz and 1402 Hz respectively. In Fig. 15 an example of the response detected by the laser scanner is shown. Considering this preliminary results, it was chosen to compare the BTT and the strain gauges measurements acquired during the rotatating tests for the 1FR and 1T family modes at $ND = 7$.

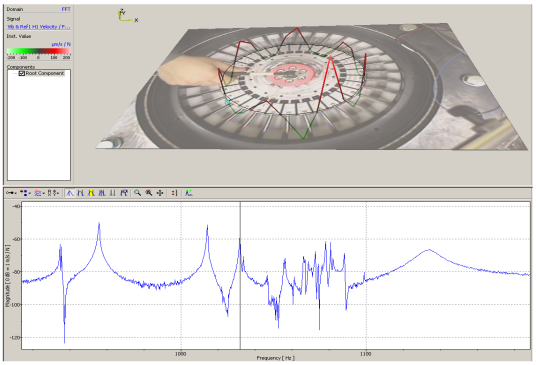

Figure 15: Hammer test on dummy disk 2: 1FR mode identification.

6.2. Test campaign on the dummy disk 2

According to Eq. 2 considering that the number of blades is $N_b = 32$, and assuming $j = 2$, it can be deduced that the mode with $ND = 7$ can be excited by an excitation with $EO = 57$. Moreover from Eq. 1 it can be derived that assuming $i = 3$ a number of equally spaced magnets $m = 19$ positioned in front of the rotating disk can produce an excitation force with $EO = 57$ in the disk. A test campaign was then performed with 19 permanent magnets (Fig. 16) at a gap of 5 mm from the blade leading edges in order to produce in the disk a travelling excitation force with $EO^3_{19} = 57$, which in a certain speed range

excites the modes at $ND = 7$.

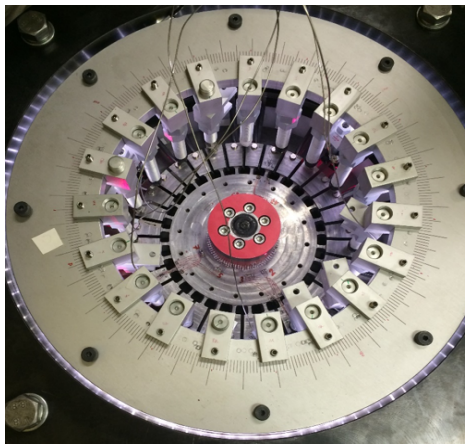

Figure 16: Dummy disk 2 excited by 19 permanent magnets.

The main tests parameters are listed in Table 5. Strain and displacement were acquired simultaneously for the 2 speed ranges (Table 5) including the values of n_{res} at which the resonances occur. For each test a linear speed sweep with an acceleration of 0.3125 Hz/s was performed. The test campaign was repeated 3 times.

Mode	*EO*	*ND*	n-range
-	-	-	rpm
1FR	57	7	1000 - 1150
1T	57	7	1350 - 1500

Table 5: Rotation speed ranges for the test campaign on the dummy disk 2.

6.3. The test results

The same procedure used for the previous disk was used to process the strain gauges signals. The displacement amplitudes in resonance obtained by the BTT were averaged over three acquisitions. Even for this disk the measured values showed high repeatability (standard deviation $\bar{\sigma} < 0.21\%$ of the mean value).

Table 6 reports the displacement amplitude values and the natural frequencies detected both by stran gauges and by the BTT system. It can be noted that in this case the value of displacement (u_{BTT} or u_{SG}) are an order of magnitude lower than those detected for the dummy disk 1 (Table 4). Even with these small displacement values the accuracy of the measurement is still good. As shown in Table 6 the difference in frequency is lower than 2.5%, and the difference in amplitude is lower than 5%.

Mode	ND	$\bar{f}_{SG}$	$\bar{f}_{BTT}$	e_f	$\bar{u}_{SG}$	$\bar{u}_{BTT}$	e_u
-	-	Hz	Hz	%	μm	μm	%
1FR	7	1029.40	1022.75	0.65	136.43	131.37	3.70
1T	7	1402.20	1368.05	2.43	155.48	162.54	4.54

Table 6: BTT-strain gauges comparison for the dummy disk 2 when the CFF method is adopted.

6.4. Nodal diameter identification on the dummy disk 2

The forced responses obtained for the mode 1T on each blade of the dummy disk 2 are plotted in Fig. 17 (a).

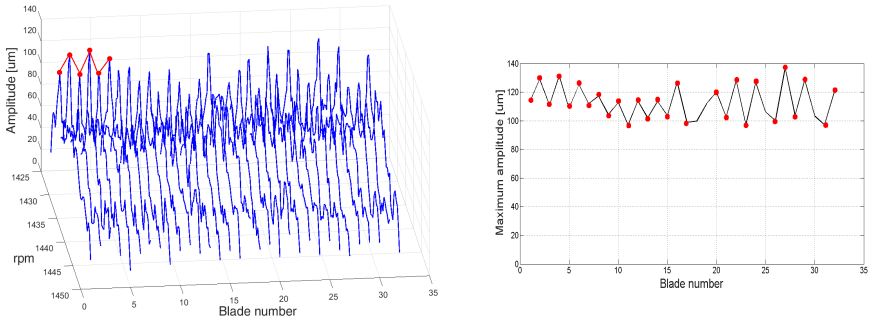

(a) (b)

Figure 17: Experimental measurements on the dummy disk 2 ($N_b = 32$) by the BTT, mode shape with $ND = 7$ mode. (a) Forced responses of all the blades, (b) spatial wave.

The low displacement amplitudes, compared to the dummy disk 1, lead to a set of more noisy data collected by the tip timing probes. It can however be observed that also in this case the phenomenon of the spatial wave can still be present as highlighted in Fig. 17 (b). The shape of the lobes is in this case quite irregular but it is still possible to recognize a modulated spatial wave with 14 peaks. In this case 14 peaks are expected since the excited traveling response is characterized by a nodal diameter $ND = 7$.

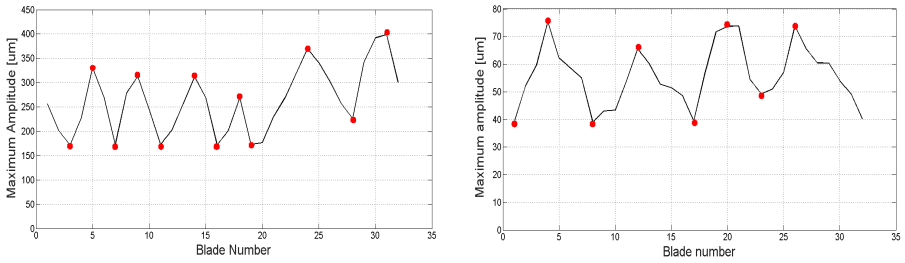

(a) (b)

Figure 18: Envelope of the maxima amplitudes of the experimental forced responses (spatial waves) for the dummy disk 2 ($N_b = 32$). (a) mode shape with $ND = 13$ and (b) $ND = 2$.

The observation of this phenomenon is confirmed by other tests. An excitation with $EO = 19$ is produced by 19 magnets. According to Eq. 2, considering the number of blades ($N_b = 32$) and $j = 1$, the engine order $EO = 19$ excites the mode with $ND = 13$. The envelope of the maxima amplitudes of the forced responses in this case is that of Fig. 18 (a) where six lobes are visible. The presence of six lobes instead of the 26 expected lobes, for the case of $ND = 13$, can be justify also here considering the aliasing Eq. 8. In fact, the number 26 of the expected lobes of the spatial waves is higher than $N_b/2$. For the aliasing the visible number of lobes is six lobes ($32 - 26 = 6$).

In order to confirm the results in one case where the aliasing phenomenon is not present, the measurement was repeated with 5 magnets. According to the Eq. 1 5 magnets produce on the blades a set of travelling forces characterized by $EO_1 5 = 15, 30, 45, \ldots$. In particular the measurement was performed by using

$EO = 30$ in order to excite, according to Eq. 2, the mode shape with $ND = 2$. The envelope of the maxima amplitudes of the forced responses in this case is that of Fig. 18 (b) where four lobes, as expected, are visible since the aliasing is not present.

7. Conclusions

In this paper a BTT system with a new concept of probes positioning was tested on two dummy disks (dummy disk 1 and dummy disk 2). The dummy disk 1 has a simple flat geometry and its blades show in resonance high displacement amplitudes (1600 - 2300 μm). The dummy disk 2 is more similar to a real turbine disk, it is characterized by families of modes close to each others.

Two key features were here presented. First, a new measurement configuration for the optical probes of a BTT system, the *beam shutter* or *beam interrupted* configuration, was tested by comparing the BTT results with the strain gauges results. The beam shutter configuration proved to work properly since it gives the expected collection of measured data from the time of arrivals of each blade under each probe. For the dummy disk 1 for the selected modes high blades displacement amplitudes (1600 - 2300 μm) were obtained with an accuracy less than 2% compared with strain gauges measurements. For the dummy disk 2 the amplitude of the displacements for the measured modes (130-150 μm) was smaller than in the previous disk. Even if the low amplitude values lead to a set of more noisy data collected by the BTT probes, the accuracy with respect to strain gauge measurements is still high (errors less than 5%). These results give confidence in this new way of positioning the optical probes. Second, a novel method to experimentally observe the nodal diameter number of the detected mode is proposed. The method takes advantage of the availability of the forced responses of all the blades typical of the BTT measurements. The method works when the detected mode is quite isolated from the other modes and in presence of small mistuning. It does not work when the mistuning is large enough to completely decouple the blade row and destroy the cyclic sym-

metry of the disk. It was proved that a small mistuning produces a spatial wave modulating the vibration amplitude of the blade row. It was then shown that the number of nodal diameter related to the main mode can be identified, starting from the number of lobes of this modulation.

8. Aknowledgments

The work described in this paper has been developed within the *GREAT 2020-2* project funded by the Italian Government.

References

[1] Zielinski, M., and G. Ziller. *Noncontact vibration measurements on compressor rotor blades*. Measurement Science and Technology 11.7 (2000): 847.

[2] Zablotskiy, I. Ye, and Yu A. Korostelev. *Measurement of resonance vibrations of turbine blades with the ELURA device*. Energomashinostroneniye,(USSR) 2 (1970): 36-39.

[3] Zielinski, Michael, and Gerhard Ziller. *Noncontact blade vibration measurement system for aero engine application*. 17th International Symposium on Airbreathing Engines. 2005.

[4] Heath, S., and M. Imregun. *An improved single-parameter tip-timing method for turbomachinery blade vibration measurements using optical laser probes*. International journal of mechanical sciences 38.10 (1996): 1047-1058.

[5] Dimitriadis, G., Carrington, I.B., Wright, J.R., and Cooper, J.E. *Blade-tip timing measurement of synchronous vibrations of rotating bladed assemblies*. Mechanical Systems and Signal Processing 16.4 (2002): 599-622.

[6] Heath, S., and M. Imregun. *A survey of blade tip-timing measurement techniques for turbomachinery vibration.* Journal of Engineering for Gas Turbines and Power 120.4 (1998): 784-791.

[7] Heath, Steve. *A new technique for identifying synchronous resonances using tip-timing.* ournal of Engineering for Gas Turbines and Power 122.2 (2000): 219-225.

[8] Carrington, I. B., Wright, J. R., Cooper, J. E., Dimitriadis, G. *A comparison of blade tip timing data analysis methods.* Proceedings of the Institution of Mechanical Engineers, Part G: Journal of Aerospace Engineering, 215(5), 301-312.

[9] Gallego-Garrido, J., Dimitriadis, G., and Wright, J.R. *A class of methods for the analysis of blade tip timing data from bladed assemblies undergoing simultaneous resonancesPart I: Theoretical development.* International Journal of Rotating Machinery, 2007.

[10] Gallego-Garrido, J., Dimitriadis, G., and Wright, J.R. *A class of methods for the analysis of blade tip timing data from bladed assemblies undergoing simultaneous resonancesPart II: Experimental Validation.* International Journal of Rotating Machinery, 2007.

[11] Knappett, D., and J. Garcia. *Blade tip timing and strain gauge correlation on compressor blades.* Proceedings of the Institution of Mechanical Engineers, Part G: Journal of Aerospace Engineering 222.4 (2008): 497-506.

[12] Berruti T., Maschio V., Calza P. *Experimental investigation on the forced response of a dummy counter-rotating turbine stage with friction damping.* Journal of Engineering for Gas Turbines and Power 134.12 (2012): 122502.

[13] Hood Technology. *Analyze Blade Vibration User Manual* (ver 7.5).

[14] C. M. Firrone, T. Berruti. *An electromagnetic system for the non-contact excitation of bladed disks.* Experimental mechanics 52.5 (2012): 447-459.